







Floquet quantum thermal transistor

Nikhil Gupta ¹, Srijan Bhattacharyya ^{1,2}, Bikash Das ³, Subhadeep Datta ³,
Victor Mukherjee ^{4,*} and Arnab Ghosh ^{1,†}

¹Indian Institute of Technology Kanpur, Kanpur, Uttar Pradesh 208016, India

²Department of Chemistry, University of Colorado, Boulder, Colorado 80309, USA

³School of Physical Sciences, Indian Association for the Cultivation of Science, 2A and B Raja S. C. Mullick Road, Jadavpur, Kolkata 700032, India

⁴Department of Physical Sciences, IISER Berhampur, Berhampur 760010, India



(Received 18 April 2022; accepted 28 June 2022; published 9 August 2022)

We apply periodic control to realize a quantum thermal transistor, which we term as the Floquet quantum thermal transistor. Periodic modulation allows us to control the heat flows and achieve large amplification factors even for fixed bath temperatures. Importantly, this transistor effect persists in the *cutoff region*, where traditional quantum thermal transistors operating in the absence of periodic modulation, fail to act as viable heat modulation devices.

DOI: [10.1103/PhysRevE.106.024110](https://doi.org/10.1103/PhysRevE.106.024110)

I. INTRODUCTION

Research on quantum machines [1–5] has received immense interest during the last decade, owing to the important role played by them in the fields of quantum thermodynamics [6–11] and quantum technologies [12,13]. Recent progress in the ability of researchers to probe and control systems in the quantum regime [14,15] have led to experimental realizations of several such machines [16–19]. The development of high-performing quantum thermal machines demands improvement in our abilities to control thermal currents at the microscopic scale. Consequently, several studies focused on modeling of quantum thermal rectifiers and quantum thermal transistors, aimed at controlling thermal currents in open quantum systems [20–25]. The above-mentioned thermal rectifiers are analogous to their electronic counterparts; they exhibit asymmetric fluxes when the temperatures at the two ends are inverted. A thermal transistor, on the other hand, regulates the heat flow between two of its terminals in response to the temperature change of a thermal bath coupled to a third terminal. Following the theoretical proposal of a thermal transistor reported in Refs. [26,27], several works addressed other types of thermal transistors, including the metal-superconductor thermal transistors [28], near-and-far-field thermal transistors [29–32], and quantum thermal transistors [22], to name a few. A significant advantage of such thermal transistors is that they can implement several thermal operations, viz. heat swap [33], heat path selector [34], and so on.

Recent works showed the possibility to realizing the thermal transistor-effect through simple quantum systems. For example, Joulain *et al.* [22] and Mandarino *et al.* [24] demonstrated transistor action with three strongly coupled

two-level systems (TLSs) interacting with their respective thermal baths. Guo *et al.* [35] identified similar transistor behavior with a three-qubit system under trilinear qubit interactions. Zhang *et al.* [34,36] demonstrated that a system of three Coulomb coupled quantum dots can also exhibit such characteristics. In Ref. [35], a coupled qubit and qutrit were shown to display transistor-action in the thermal domain, while Majland *et al.* [23] extended it further with superconducting circuits. With an external optical field, the concept of field effect quantum transistor and Darlington transistor were proposed by Wijesekara *et al.* [25].

Most of the works on quantum thermal transistors till now focused on realizing the transistor effect through changes in bath temperatures [22,24,27,32,36–39]. In contrast, in this paper we apply quantum control to realize a model of a *Floquet quantum thermal transistor* (FQT); here we achieve the transistor effect through periodic modulation of the system Hamiltonian. This periodic modulation allows us to control the heat currents even for fixed bath temperatures. Most importantly, the present control scheme enables us to achieve the transistor effect even in the so-called *cutoff regime*, where traditional quantum thermal transistors, which depend on a variation of bath temperatures, fail to perform.

The present work is organized as follows. We introduce the model, dynamics, and thermal currents in Sec. II. Section III A deals with general transistor characteristics. We give a comparison with an unmodulated quantum thermal transistor in Sec. III B, consider FQT at arbitrary temperatures in Sec. III C, and the low-temperature limit in Sec. III D. Finally, we conclude in Sec. IV. We include technical details in the Appendixes.

II. MODEL AND DYNAMICS

Quantum thermal transistors are analogous to their electronic counterparts, with temperatures replacing voltages and thermal energy flows replacing electric currents [22].

*mukherjeev@iiserbpr.ac.in

†arnab@iitk.ac.in

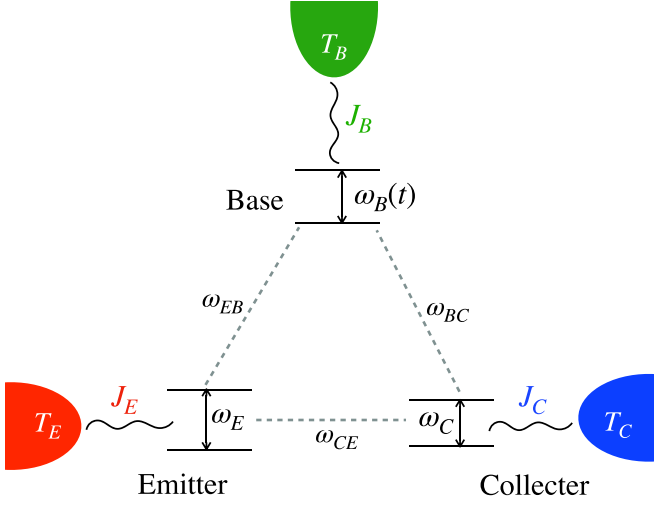


FIG. 1. Schematic diagram of the FQT model system. The three terminals (qubits) are coupled to three thermal baths. We achieve thermal transistor effect through periodic modulation of the frequency $\omega_B(t)$ of the base qubit.

Quantum thermal transistors are typically three-terminal devices, with the channels coupled to their respective thermal baths (see Fig. 1). Heat current enters the setup through one terminal [termed as the *emitter* (E)] and leaves through the remaining two terminals [termed as the *base* (B) and the *collector* (C)]. The transistor effect is said to be obtained when a small thermal current at the base can be used to control large collector and emitter currents, which can also be modulated, switched, and amplified by small changes in the base current. Previous works studied the modulation of J_B through (i) the variation of base temperature as in the case of quantum thermal transistors [22] or (ii) by the application of the external optical field as in the case of field effect quantum transistors [25]. In contrast, here we shall do the same through periodic modulation of the base terminal frequency. Remarkably, as we discuss below, this periodic modulation allows us to achieve the transistor effect even in regimes hitherto considered to be unfavorable for transistor operation. We note that here we use the sign convention that the thermal currents which enter (leave) the system are positive (negative).

We model the FQT through three interacting TLSs, representing the three terminals. As shown in Fig. 1, the α th TLS is coupled to a thermal reservoir at temperature T_α ($\alpha = E, B, C$). Similar to the authors of Ref. [22], we consider T_E and T_C to be fixed; T_B can vary and $T_E > T_B, T_C$. The Hamiltonian of the entire setup is then given by three terminals FQT system as

$$\begin{aligned}
 H(t) &= H_S(t) + H_R + H_I, \\
 H_S(t) &= \frac{\hbar\omega_E}{2}\sigma_z^E + \frac{\hbar\omega_B(t)}{2}\sigma_z^B + \frac{\hbar\omega_C}{2}\sigma_z^C + \frac{\hbar\omega_{EB}}{2}\sigma_z^E\sigma_z^B \\
 &\quad + \frac{\hbar\omega_{BC}}{2}\sigma_z^B\sigma_z^C + \frac{\hbar\omega_{CE}}{2}\sigma_z^C\sigma_z^E, \\
 H_R &= H_{RC} + H_{RB} + H_{RE}, \\
 H_I &= \sigma_x^C \otimes \mathcal{R}_C + \sigma_x^B \otimes \mathcal{R}_B + \sigma_x^E \otimes \mathcal{R}_E.
 \end{aligned} \tag{1}$$

Here $H_S(t)$ denotes the Hamiltonian describing the three TLSs, σ_θ^α is the Pauli matrix along dimension θ ($= x, y, z$) acting on the terminal α ($= E, B, C$), ω_α refers to the frequency of the respective TLS, whereas $\omega_{\alpha\alpha'}$ denotes the interaction strength between the α and α' terminals. We assume that the base terminal is periodically modulated at a frequency $\nu = \frac{2\pi}{\tau}$ such that

$$\omega_B(t + \tau) = \omega_B(t), \quad \frac{1}{\tau} \int_t^{t+\tau} \omega_B(t) dt = \omega_0. \tag{2}$$

Here ω_0 denotes the time-averaged frequency of B .

The eigenstates of $H_S(t)$, labeled by $|1\rangle = |\uparrow\uparrow\uparrow\rangle$, $|2\rangle = |\uparrow\uparrow\downarrow\rangle$, $|3\rangle = |\uparrow\downarrow\uparrow\rangle$, $|4\rangle = |\uparrow\downarrow\downarrow\rangle$, $|5\rangle = |\downarrow\uparrow\uparrow\rangle$, $|6\rangle = |\downarrow\uparrow\downarrow\rangle$, $|7\rangle = |\downarrow\downarrow\uparrow\rangle$, and $|8\rangle = |\downarrow\downarrow\downarrow\rangle$ [22], are obtained through the tensor product of the σ_z^α eigenstates, $|\uparrow\rangle$ and $|\downarrow\rangle$ of the individual TLS (see Appendix A). $H_{R\alpha}$ denotes the Hamiltonian of the thermal bath coupled to the terminal α , through the term $\sigma_x^\alpha \otimes \mathcal{R}_\alpha$ included in the interaction Hamiltonian H_I ; \mathcal{R}_α is an operator acting on the bath α .

The above interaction imposes a restriction on flipping more than one spin at a time. Consequently, there are, in total, 12 allowed transitions. The base reservoir induces the four transitions between $1 \leftrightarrow 3$, $2 \leftrightarrow 4$, $5 \leftrightarrow 7$, and $6 \leftrightarrow 8$, while the emitter bath drives the transitions $1 \leftrightarrow 5$, $2 \leftrightarrow 6$, $3 \leftrightarrow 7$, and $4 \leftrightarrow 8$, and the collector bath triggers the transitions $1 \leftrightarrow 2$, $3 \leftrightarrow 4$, $5 \leftrightarrow 6$, and $7 \leftrightarrow 8$. The rates at which the above transitions occur can be computed using the Floquet-Lindblad master equation [6,9,40,41].

One can use the Floquet method and implement the Born, Markov, and secular approximations to arrive at the time-independent Lindblad dissipators describing the time evolution of the density matrix ρ for the state of the FQT, given by

$$\frac{d\rho}{dt} = \mathcal{L}_E[\rho] + \tilde{\mathcal{L}}_B[\rho] + \mathcal{L}_C[\rho]. \tag{3}$$

Here the Lindbladians are given by (see Appendix A)

$$\begin{aligned}
 \mathcal{L}_\alpha[\rho] &= \sum_{\{\Omega_\alpha\}} [G_\alpha(\Omega_\alpha)\mathcal{D}(A_\alpha)[\rho] \\
 &\quad + G_\alpha(-\Omega_\alpha)\mathcal{D}(A_\alpha^\dagger)[\rho]], \quad \alpha \in \{E, C\}, \\
 \tilde{\mathcal{L}}_B[\rho] &= \sum_{\{\Omega_B\}} \sum_{q \in \mathbb{Z}} \mathcal{L}_B^q[\rho], \\
 \mathcal{L}_B^q[\rho] &= P_q [G_B(\Omega_B + q\nu)\mathcal{D}(A_B)[\rho] \\
 &\quad + G_B(-\Omega_B - q\nu)\mathcal{D}(A_B^\dagger)[\rho]],
 \end{aligned} \tag{4}$$

in terms of the dissipater

$$\mathcal{D}(A_\alpha)[\rho] = A_\alpha \rho A_\alpha^\dagger - \frac{1}{2}[\rho, A_\alpha^\dagger A_\alpha]. \tag{5}$$

The operator A_α assumes the form $|i\rangle\langle j|$ ($i \neq j$; $i, j = 1, 2, \dots, 8$), and causes the 12 transitions described above with positive frequency $\Omega_\alpha = \omega_{ij}^\alpha$, between the eigenstates $|i\rangle$ and $|j\rangle$ with frequency difference ω_{ij} , subject to the constraint of four allowed transitions corresponding to the terminal α . Here $q \in \mathbb{Z}$ denotes the different Floquet modes with frequencies $\Omega_B + q\nu$ and amplitudes P_q ($P_q = P_{-q}$, $\sum_{q \in \mathbb{Z}} P_q = 1$). $G_\alpha(\omega) = G_0(\omega)[1 + \tilde{n}_\alpha(\omega)]$ is the spectral function of the bosonic bath coupled to the terminal α , where $G_0(\omega)$ is the

spontaneous-emission rate and $\bar{n}_\alpha(\omega) = [\exp \frac{\hbar\omega}{k_B T_\alpha} - 1]^{-1}$ is the thermal population of the bath mode at frequency ω and temperature T_α [6,42–45].

The Floquet-Lindblad master Eq. (3) shows that the TLS base system effectively acts as a multilevel system, with the different energy gaps given by the Floquet modes q . The master Eq. (3) drives the system toward a Gibbs-like steady state, characterized by the different effective energy gaps, the amplitudes P_q , and the spectral functions and temperatures of the baths (see Appendix A).

The steady state $\rho = \rho_{ss}$, defined by the condition $\dot{\rho}_{ss} = 0$, is diagonal in the energy eigenbasis $|j\rangle$ ($j = 1, 2, \dots, 8$), such that Eq. (3) reduces to

$$\begin{aligned} \dot{\rho}_{11} = 0 &= \Gamma_{51}^E + \tilde{\Gamma}_{31}^B + \Gamma_{21}^C, \\ \dot{\rho}_{22} = 0 &= \Gamma_{62}^E + \tilde{\Gamma}_{42}^B + \Gamma_{12}^C, \\ \dot{\rho}_{33} = 0 &= \Gamma_{73}^E + \tilde{\Gamma}_{13}^B + \Gamma_{43}^C, \\ \dot{\rho}_{44} = 0 &= \Gamma_{84}^E + \tilde{\Gamma}_{24}^B + \Gamma_{34}^C, \\ \dot{\rho}_{55} = 0 &= \Gamma_{15}^E + \tilde{\Gamma}_{75}^B + \Gamma_{65}^C, \\ \dot{\rho}_{66} = 0 &= \Gamma_{26}^E + \tilde{\Gamma}_{86}^B + \Gamma_{56}^C, \\ \dot{\rho}_{77} = 0 &= \Gamma_{37}^E + \tilde{\Gamma}_{57}^B + \Gamma_{87}^C, \\ \dot{\rho}_{88} = 0 &= \Gamma_{48}^E + \tilde{\Gamma}_{68}^B + \Gamma_{78}^C. \end{aligned} \quad (6)$$

Here the net transition rates are defined by the following terms:

$$\begin{aligned} \Gamma_{ij}^\alpha &= G_\alpha(\omega_{ij})\rho_{ii} - G_\alpha(-\omega_{ij})\rho_{jj}, \quad \alpha \in \{E, C\}, \\ \tilde{\Gamma}_{ij}^B &= \sum_q \Gamma_{ij,q}^B, \end{aligned} \quad (7)$$

where

$$\begin{aligned} \Gamma_{ij,q}^B &= P_q [G_B(\omega_{ij} + q\nu)\rho_{ii} - G_B(-\omega_{ij} - q\nu)\rho_{jj}], \\ \Gamma_{ij}^{E(C)} &= -\Gamma_{ji}^{E(C)}, \quad \tilde{\Gamma}_{ij}^B = -\tilde{\Gamma}_{ji}^B. \end{aligned} \quad (8)$$

For simplicity, here, we choose the baths to be Ohmic, so the spectral functions are linear with $G_0(\omega) = \kappa\omega$, where the constant κ is the same for all three reservoirs.

Finally, one can use the Spohn inequality [46] and the dynamical version of the second law of thermodynamics [43] to arrive at the explicit expressions for the steady state heat currents (see Appendix B)

$$\begin{aligned} J_{E(C)} &= -\hbar \sum_{\omega_{ij}} \omega_{ij} \Gamma_{ij}^{E(C)}, \\ J_B &= -\hbar \sum_q \sum_{\omega_{ij}} (\omega_{ij} + q\nu) \Gamma_{ij,q}^B. \end{aligned} \quad (9)$$

III. TRANSISTOR CHARACTERISTICS

A. General results

The gain of a thermal transistor can be quantified through dynamical amplification parameters

$$\beta_+ = \frac{\partial J_C}{\partial J_B}, \quad \beta_- = \frac{\partial J_E}{\partial J_B}. \quad (10)$$

Large values of β_\pm imply high amplifications, which may even diverge for J_B passing through a minimum. We note that

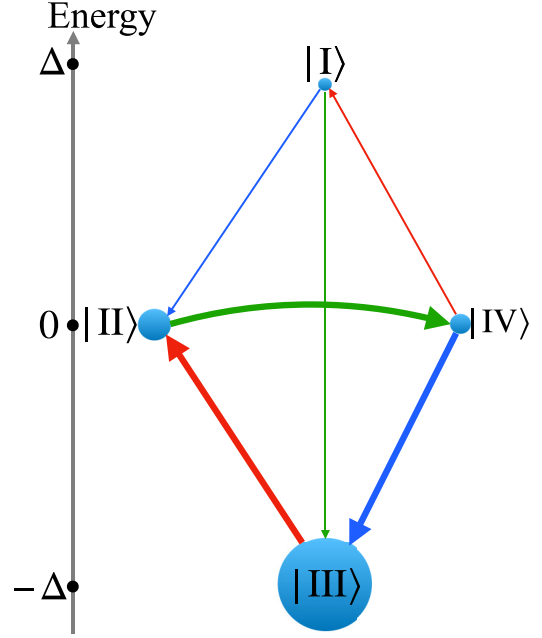


FIG. 2. Energy levels for $\omega_E = \omega_0 = \omega_C = 0$, $\omega_{EC} = 0$, and $\omega_{EB} = \omega_{BC} = \Delta$. The arrows indicate the net decaying rates Γ_{i-j}^α between the states $|I\rangle$, $|II\rangle$, $|III\rangle$, and $|IV\rangle$ due to bath E (red), bath B (green), and bath C (blue).

conservation of energy demands $J_B + J_E + J_C = 0$, which in turn results in the relation $\beta_+ + \beta_- = -1$; here $J_E > 0$ and $J_B, J_C < 0$ in resemblance with the common base electronic transistor [47].

Let us now look into the details of the dynamics that allow us to operate the FQT with high β_\pm . To devise a common-base FQT, we set the emitter-collector coupling ω_{EC} to be zero, while the emitter-base and base-collector couplings are taken to be nonzero and equal, i.e., $\omega_{EB} = \omega_{BC} = \Delta$ and [see Eq. (1) and Appendix C]. Note that, if the coupling between all three qubits is equal (symmetric), then the transistor effect disappears. Although one may achieve a thermal transistor effect with asymmetric couplings and nonzero qubit frequencies as well (for details see Ref. [22]). However, to reduce the number of the states and avoid numerical complexity we set bare frequencies of all the TLSs as zero, i.e., $\omega_C = \omega_E = \omega_0 = 0$. Under this choice of parameter, some of the eigenstates become degenerate, so that we are finally left with only three distinct energy levels. We rename the states $|1\rangle$ and $|8\rangle$ as $|I\rangle$, $|2\rangle$ and $|7\rangle$ as $|II\rangle$, $|3\rangle$ and $|6\rangle$ as $|III\rangle$, and $|4\rangle$ and $|5\rangle$ as $|IV\rangle$ (Fig. 2). Similarly, we introduce new density matrix elements as $\rho_I = \rho_{11} + \rho_{88}$, $\rho_{II} = \rho_{22} + \rho_{77}$, $\rho_{III} = \rho_{33} + \rho_{66}$, and $\rho_{IV} = \rho_{44} + \rho_{55}$. Introducing the net decaying rates Γ_{i-j}^α ($\alpha = E, B, C$; $i, j = I, II, III, IV$) between these states (see Appendix C) following Eq. (9), the three currents can be written as

$$\begin{aligned} J_E &= -\hbar\Delta [\Gamma_{I-IV}^E + \Gamma_{II-III}^E], \\ J_B &= -\hbar \sum_{q=0,\pm 1} (2\Delta + q\nu) \Gamma_{I-III,q}^B, \\ J_C &= -\hbar\Delta [\Gamma_{I-II}^C + \Gamma_{IV-III}^C]. \end{aligned} \quad (11)$$

where

$$\begin{aligned}
 \Gamma_{I-IV}^E &= \kappa \Delta \{ \rho_I - e^{-\hbar\Delta/k_B T_E} \rho_{IV} \}, \\
 \Gamma_{II-III}^E &= \kappa \Delta \{ \rho_{II} - e^{-\hbar\Delta/k_B T_E} \rho_{III} \}, \\
 \Gamma_{IV-III}^C &= \kappa \Delta \{ \rho_{IV} - e^{-\hbar\Delta/k_B T_C} \rho_{III} \}, \\
 \Gamma_{I-II}^C &= \kappa \Delta \{ \rho_I - e^{-\hbar\Delta/k_B T_C} \rho_{II} \}, \\
 \Gamma_{I-III,q}^B &= P_q (2\Delta + q\nu) \{ \rho_I - e^{-\hbar(2\Delta+q\nu)/k_B T_B} \rho_{III} \}. \quad (12)
 \end{aligned}$$

To ensure that the system dynamics fulfills the Born-Markov approximations, the system relaxation time Γ^{-1} must be larger than the characteristic timescale associated with the system frequency, i.e., Δ^{-1} . As we show in Appendix C, level decaying rates exhibit significant enhancement with the increase of base temperature, which indicates that the Born-Markov approximation may no longer be a good approximation at high temperature limits. As a result, we choose the highest temperature T_E such that $e^{-\hbar\Delta/k_B T_E} \ll 1$.

Transitions between the different states of FQT are illustrated in Fig. 2. The arrows denote the transition directions whereas larger widths indicate higher decay rates Γ_{i-j}^α . As shown in Fig. 2, the energy exchanges are primarily dominated by the $III-II$ and $IV-III$ transitions. Consequently, one expects $J_E, J_C \gg J_B$ [see Eq. (11)]. These observations can be explained by examining carefully the following populations and heat current expressions. If we limit our calculation in the leading orders of $e^{-\hbar\Delta/k_B T_E}$ and the first two harmonics of the modulation (i.e., $|q| = 0, 1$), we can evaluate the approximate form of the populations (see Appendix C for a detailed derivation) as

$$\begin{aligned}
 \rho_I &\simeq \frac{1}{2(1 + P_0 + 2P_1)} \\
 &\times \frac{P_0 k_B T_B + P_1 \hbar \nu \left(\frac{e^{\hbar\nu/k_B T_B} + 1}{e^{\hbar\nu/k_B T_B} - 1} \right)}{2P_0 k_B T_B + 2P_1 \hbar \nu \left(\frac{e^{\hbar\nu/k_B T_B} + 1}{e^{\hbar\nu/k_B T_B} - 1} \right) + \hbar\Delta} e^{-2\hbar\Delta/k_B T_E}, \\
 \rho_{II} &\simeq \frac{P_0 k_B T_B + P_1 \hbar \nu \left(\frac{e^{\hbar\nu/k_B T_B} + 1}{e^{\hbar\nu/k_B T_B} - 1} \right) + \hbar\Delta}{2P_0 k_B T_B + 2P_1 \hbar \nu \left(\frac{e^{\hbar\nu/k_B T_B} + 1}{e^{\hbar\nu/k_B T_B} - 1} \right) + \hbar\Delta} e^{-\hbar\Delta/k_B T_E}, \\
 \rho_{III} &\simeq 1 - e^{-\hbar\Delta/k_B T_E}, \\
 \rho_{IV} &\simeq \frac{P_0 k_B T_B + P_1 \hbar \nu \left(\frac{e^{\hbar\nu/k_B T_B} + 1}{e^{\hbar\nu/k_B T_B} - 1} \right)}{2P_0 k_B T_B + 2P_1 \hbar \nu \left(\frac{e^{\hbar\nu/k_B T_B} + 1}{e^{\hbar\nu/k_B T_B} - 1} \right) + \hbar\Delta} e^{-\hbar\Delta/k_B T_E}. \quad (13)
 \end{aligned}$$

To obtain the above set of closed form analytical expressions, we take for simplicity $T_C, T_B \ll T_E$ so that we can neglect the contribution of $e^{-\hbar\Delta/k_B T_C}$ and $e^{-\hbar\Delta/k_B T_B}$ with regard to (w.r.t.) $e^{-\hbar\Delta/k_B T_E}$ in the populations' expressions. Using Eqs. (11) to (13), we now explicitly evaluate the three thermal currents as

$$\begin{aligned}
 J_E &\simeq -J_C \simeq \kappa \hbar \Delta^2 \rho_{IV}, \\
 J_B &\simeq \kappa \hbar \sum_{q=0,\pm 1} P_q (2\Delta + q\nu)^2 [e^{-\hbar(2\Delta+q\nu)/k_B T_B} - \rho_I]. \quad (14)
 \end{aligned}$$

We note that J_E and J_C are driven by ρ_{IV} , i.e., the state populations at the intermediate energy levels. On the other hand, J_B is determined by the population ρ_I of the most energetic states, with all spins aligned parallel. As we can see from

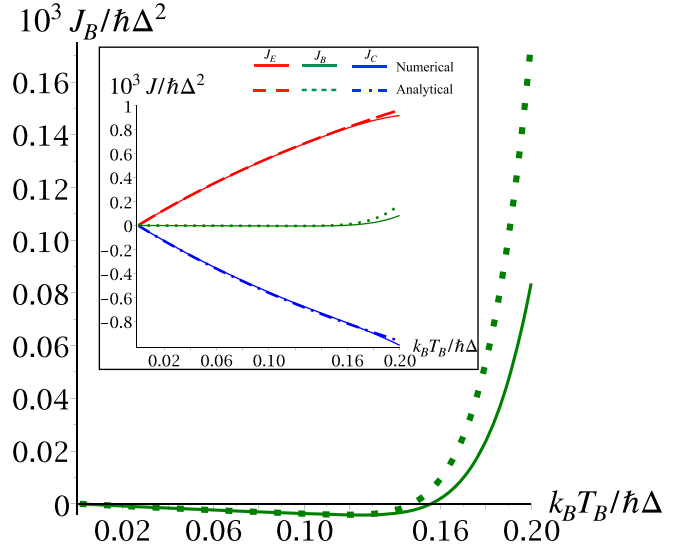


FIG. 3. Thermal current J_B versus $k_B T_B / \hbar \Delta$ for the unmodulated case. Solid lines indicate numerical results, while dotted lines are approximate analytical results [cf. Eq. (16)]. Inset: Thermal currents J_E, J_B , and J_C versus $k_B T_B / \hbar \Delta$ for unmodulated case with parameters, $\omega_E = \omega_0 = \omega_C = 0$, $\omega_{EC} = 0$, $\omega_{EB} = \omega_{BC} = \Delta$, $k_B T_E = 0.2\hbar\Delta$, and $k_B T_C = 0.02\hbar\Delta$.

Eq. (13), we have $\rho_I \ll \rho_{IV}$ in the limit of $k_B T_E \ll \hbar\Delta$ (see Appendix C). This in turn leads to $J_B \ll J_E, J_C$. Furthermore, as seen from Eqs. (13) and (14), we can control the populations and consequently the heat currents through control of the modulation frequency ν . In what follows, we consider different choices of the parameters that allow us to operate the FQT in the following three regimes discussed below.

B. Unmodulated quantum thermal transistor

In the absence of modulation, i.e., upon setting the limit $\nu \rightarrow 0$ and taking $P_q = \delta_{q,0}$ in Eqs. (13) and (14), we qualitatively reproduce the results reported in Ref. [22] for the populations and heat currents. Throughout our calculation we chose $\kappa = 1$. In this limit we get

$$\begin{aligned}
 \rho_I &\simeq \frac{k_B T_B}{8k_B T_B + 4\hbar\Delta} e^{-2\hbar\Delta/k_B T_E}, \\
 \rho_{II} &\simeq \frac{k_B T_B + \hbar\Delta}{2k_B T_B + \hbar\Delta} e^{-\hbar\Delta/k_B T_E}, \\
 \rho_{III} &\simeq 1 - e^{-\hbar\Delta/k_B T_E}, \\
 \rho_{IV} &\simeq \frac{k_B T_B}{2k_B T_B + \hbar\Delta} e^{-\hbar\Delta/k_B T_E}, \quad (15)
 \end{aligned}$$

and

$$\begin{aligned}
 J_E &\simeq -J_C \simeq \kappa \hbar \Delta^2 \rho_{IV}, \\
 J_B &\simeq 4\kappa \hbar \Delta^2 [e^{-2\hbar\Delta/k_B T_B} - \rho_I]. \quad (16)
 \end{aligned}$$

Apart from a negligible contribution of the order of $e^{-2\hbar\Delta/k_B T_B}$, the populations and heat currents in Eqs. (15) and (16) are identical to those reported in Ref. [22], and they match the numerical results exactly, except for $T_B \rightarrow T_E$ (see Fig. 3 and Appendix C). As expected, $|J_B| \ll |J_E|, |J_C|$; a

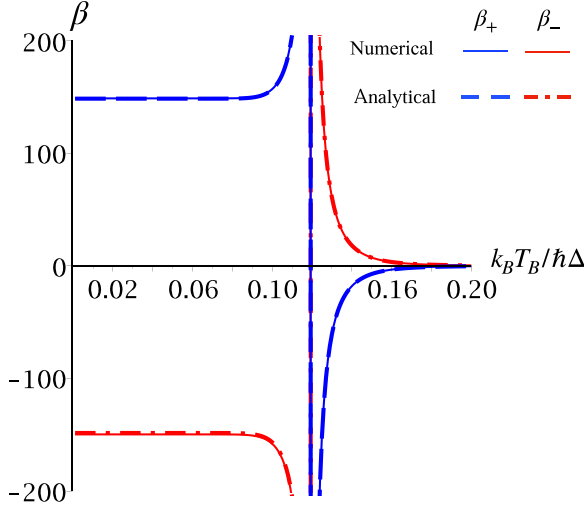


FIG. 4. Dynamical amplification factors [cf. (10)] β_+ and β_- versus $k_B T_B / \hbar \Delta$ for the unmodulated case with parameters $\omega_E = \omega_0 = \omega_C = 0$, $\omega_{CE} = 0$, $\omega_{EB} = \omega_{BC} = \Delta$, $k_B T_E = 0.2 \hbar \Delta$, and $k_B T_C = 0.02 \hbar \Delta$.

small change of J_B can significantly alter the values of J_E and J_C , thus resulting in large values of the dynamical amplification factors β_+ and β_- , as shown in Fig. 4. From Eq. (16), one can estimate that as long as T_B is not comparable to T_E , the absolute value of the dynamical amplification factors are approximately $|\beta_{\pm}| \approx e^{\hbar \Delta / k_B T_E}$. For the present choice of system parameters $\hbar \Delta / k_B T_E = 5$, the setup yields a transistor gain $\beta_{\pm} \sim e^5 \approx 150$ (Fig. 4), which corroborates with our numerical findings. Finally, we note that J_C , J_E , and J_B all tend to vanish in the limit $T_B \rightarrow 0$, so that the transistor remains in the so-called *cutoff* regime and the device stops operating as a viable heat current modulator.

C. Sinusoidal and π -flip modulations

We now study the operation of the FQT in presence of periodic modulations of $\omega_B(t)$. In particular, we consider sinusoidal and π -flip modulations, as discussed below.

1. Sinusoidal modulation

Here we consider the modulation form

$$\omega_B(t) = \omega_0 + \lambda \nu \sin(\nu t). \quad (17)$$

The condition $0 \leq \lambda \leq 1$ allows us to limit our analysis to only the first two harmonics $q = 0, \pm 1$ in Eqs. (13) and (14) [48]

$$P_0 = 1 - \frac{\lambda^2}{2}, \quad P_{\pm 1} = \frac{\lambda^2}{4}. \quad (18)$$

2. π -flip modulation

Periodic π - phase shifts modulation in the form of two alternating pulses per period [42]

$$\omega(t) = \omega_0 + \pi \sum_{n \in \mathbb{Z}} \delta[t - (n + 1/4)] - \delta[t - (n + 3/4)], \quad (19)$$

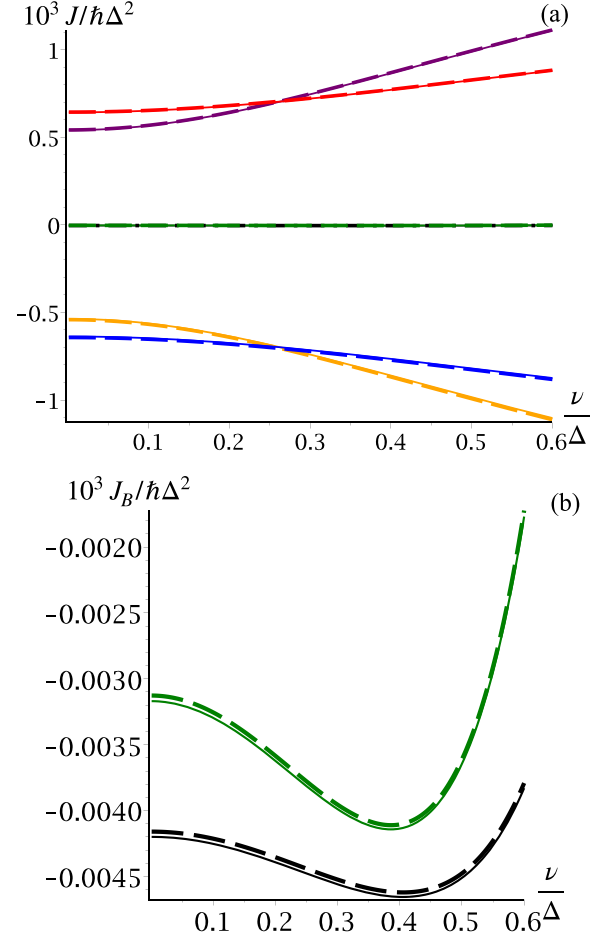


FIG. 5. (a) Thermal currents J_E , J_B , and J_C versus ν/Δ under sinusoidal modulation [J_E (red), J_B (black), and J_C (blue)] and π -flip modulation [J_E (purple), J_B (green), and J_C (orange)]. (b) Thermal current J_B versus ν/Δ for sinusoidal (black) and π -flip modulation (green). Solid lines indicate numerical values and dashed lines are approximate values of heat currents for the parameter set $\omega_E = \omega_0 = \omega_C = 0$, $\omega_{EC} = 0$, $\omega_{EB} = \omega_{BC} = \Delta$, $k_B T_E = 0.2 \hbar \Delta$, $k_B T_B = 0.118 \hbar \Delta$, $k_B T_C = 0.02 \hbar \Delta$, and $\lambda = 0.8$.

gives rise to only two leading harmonics $q = \pm 1$, with the corresponding amplitudes of the Floquet modes given by [48]

$$P_{\pm 1} \approx (2/\pi)^2. \quad (20)$$

In this case $P_0 = 0$. The results for sinusoidal and π -flip modulations are shown in Fig. 5. As we can infer from Eqs. (13) and (14), in comparison to sinusoidal modulation, the vanishing P_0 for pi-pulse results in larger values of β_{\pm} due to higher slopes in the heat currents (Figs. 5 and 6).

D. Generic modulation with $T_B \rightarrow 0$

We now emphasize the crucial advantage offered by the FQT model proposed here. As we show below, in contrast to the previously studied models of quantum thermal transistors [22,24,35,36], FQT can operate as a thermal current amplifying device in the otherwise cutoff regime of the base temperature T_B approaching zero. In this limit the populations

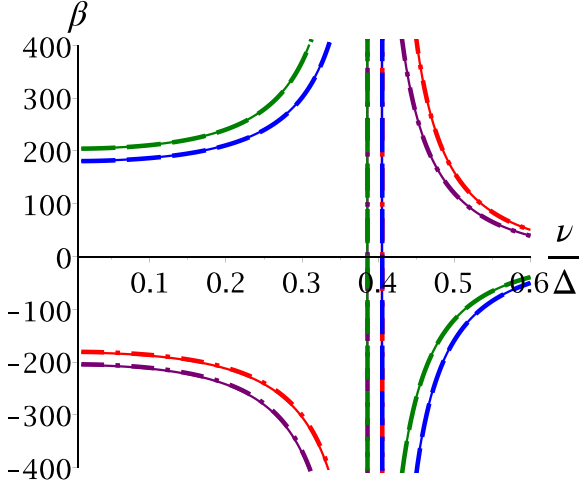


FIG. 6. Dynamical amplification factors [cf. (10)] β_+ and β_- versus ν/Δ for sinusoidal [β_+ (blue) and β_- (red)] and π -flip modulation [β_+ (green) and β_- (purple)]. Solid lines show numerical results, while dashed-dot and dashed lines correspond to approximate analytical value of β_{\pm} for the parameter set $\omega_E = \omega_0 = \omega_C = 0$, $\omega_{CE} = 0$, $\omega_{EB} = \omega_{BC} = \Delta$, $k_B T_E = 0.2\hbar\Delta$, $k_B T_C = 0.02\hbar\Delta$, $k_B T_B = 0.118\hbar\Delta$, and $\lambda = 0.8$.

and heat currents of the FQT reduce to [see Eqs. (13) and (14)]

$$\begin{aligned}\rho_I &\simeq \frac{1}{2(1+P_0+2P_1)} \frac{P_1\nu}{2P_1\nu+\Delta} e^{-2\hbar\Delta/k_B T_E}, \\ \rho_{II} &\simeq \frac{P_1\nu+\Delta}{2P_1\nu+\Delta} e^{-\hbar\Delta/k_B T_E}, \\ \rho_{III} &\simeq 1 - e^{-\hbar\Delta/k_B T_E}, \\ \rho_{IV} &\simeq \frac{P_1\nu}{2P_1\nu+\Delta} e^{-\hbar\Delta/k_B T_E},\end{aligned}\quad (21)$$

and

$$\begin{aligned}J_E &\simeq -J_C \simeq \kappa \hbar \Delta^2 \rho_{IV}, \\ J_B &\simeq -\kappa \hbar \rho_I \sum_{q=0,\pm 1} P_q (2\Delta + q\nu)^2.\end{aligned}\quad (22)$$

Clearly the nonzero Floquet amplitude P_1 , which is a direct consequence of the modulation, results in nonzero ρ_I , and therefore allows us to operate the FQT with nonzero heat currents even for $T_B \rightarrow 0$. As before, we again focus on sinusoidal and π -flip modulations to exemplify the advantage offered by the FQT. We plot the heat currents for sinusoidal and π -flip modulations in Fig. 7. As expected from Eq. (22), sinusoidal and π -flip modulations result in large amplification factors even in this regime (Fig. 8).

IV. CONCLUSION

We proposed operating quantum thermal transistors in the presence of periodic modulations, and termed the setup as Floquet quantum thermal transistors. In previously studied quantum thermal transistors, the transistor effect was realized through changes in temperature T_B of the bath coupled to the base [22,24,27,32,36–39]. This can be expected to be an energy-intensive process; a change δT_B in temperature would

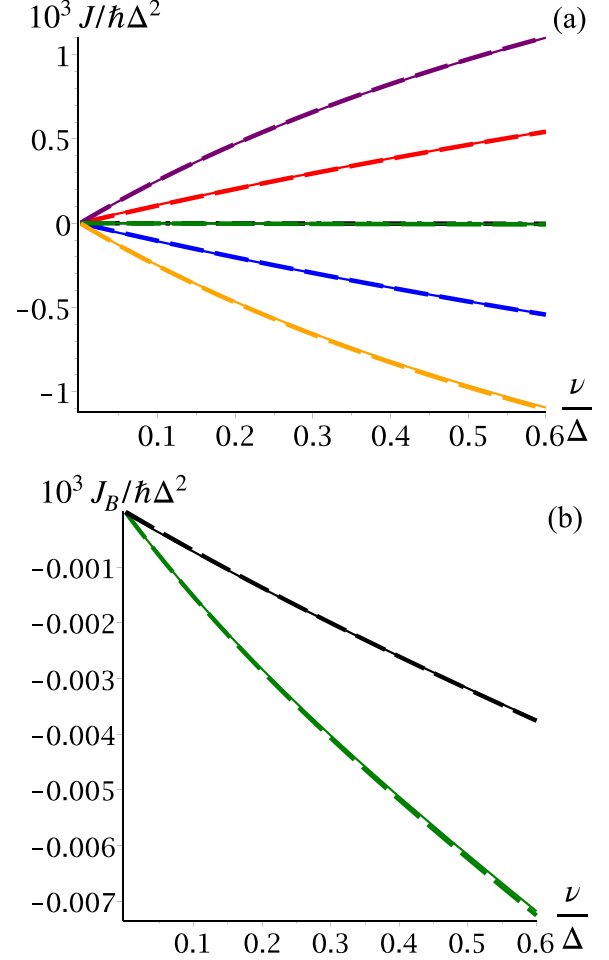


FIG. 7. (a) Thermal currents J_E , J_B , and J_C versus ν/Δ under sinusoidal modulation [J_E (red), J_B (black), and J_C (blue)] and π -flip modulation [J_E (purple), J_B (green), and J_C (orange)]. (b) Thermal current J_B versus ν/Δ for sinusoidal (black) and π -flip modulations (green), for $T_B \rightarrow 0$. Solid lines represent numerical values and dashed lines stand for approximate analytical values of heat currents for the parameter set $\omega_E = \omega_0 = \omega_C = 0$, $\omega_{EC} = 0$, $\omega_{EB} = \omega_{BC} = \Delta$, $k_B T_E = 0.2\hbar\Delta$, $k_B T_C = 0.02\hbar\Delta$, and $\lambda = 0.8$.

require a heat energy $\delta Q_B = C_B \delta T_B$, which can be large for a large heat capacity C_B of the bath. On the other hand, the periodic modulation scheme implemented here allows us to modulate the heat currents also in the presence of fixed bath temperatures. We note that the cost of periodic modulation is an interesting question as well, which we plan to address in future work. We exemplified our generic theory using sinusoidal and π -flip modulations. The crucial advantage of the FQT is its ability to operate as a heat modulation device with high amplification factors even in the traditional cutoff regime of $T_B \rightarrow 0$. This advantage stems from nonzero Floquet amplitudes P_1 , which vanish in absence of modulation. Although we use Ohmic bath spectral density throughout our calculations, we may expect a transistor effect yet in the presence of a non-Ohmic bath spectrum (such as Lorentzian), as long as the basic energy level diagram (Fig. 2) characterized by net decaying rates fulfills $J_B \ll J_E, J_C$. However, a complete

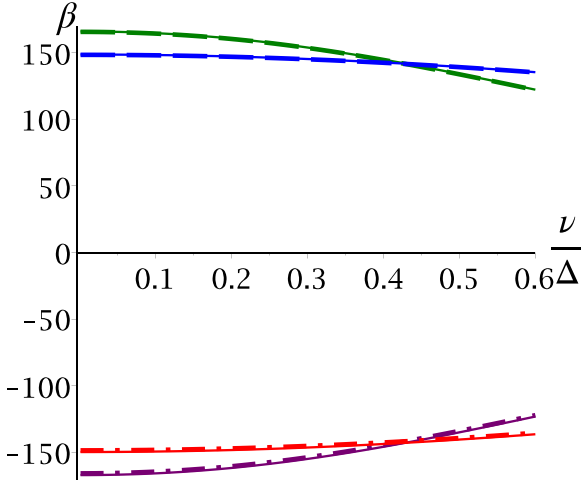


FIG. 8. Dynamical amplification factors [cf. (10)] β_+ and β_- versus ν/Δ for sinusoidal [β_+ (blue) and β_- (red)] and π -flip modulations [β_+ (green) and β_- (purple)], for $T_B \rightarrow 0$. Solid lines represent numerical values, dashed-dot and dashed lines correspond to approximate analytical values of β_{\pm} for the parameter set $\omega_E = \omega_0 = \omega_C = 0$, $\omega_{CE} = 0$, $\omega_{EB} = \omega_{BC} = \Delta$, $k_B T_E = 0.2\hbar\Delta$, $k_B T_C = 0.02\hbar\Delta$, and $\lambda = 0.8$.

analysis in the presence of a generic non-Ohmic bath is non-trivial and beyond the scope of the present work.

The experimental realization of controlled heat currents can be envisaged in a variety of physical platforms: (i) quantum thermal transistor design was predicted and realized in on-chip superconducting qubits [49]; (ii) a quantum heat engine was realized with the spin-1/2 of the ^{13}C nucleus [50]; (iii) micro and nanoelectromechanical systems (MEMS/NEMS) were used to implement nonequilibrium reservoir engineering [17]; and so on. Most of these quantum technology devices require sophisticated lithographic techniques (few tens of nanometers) and low temperature measurements. In our approach, the experimental feasibility relies on the periodic modulation of the base bath (ultrathin film) in conventional electronic bipolar junction transistor (BJT) architecture. Recent analytical results on far-field radiative heat transport concerns thermal transistor (BJT) setup where 1- μm -thick block of vanadium dioxide (VO_2), as the base, was excited with a laser with a modulation frequency of 0.5 Hz [51,52]. Interestingly, thermal rectification was achieved due to the insulator-to-metal transition of VO_2 at around 340 K, which can thus set the temperature scale of a typical base bath. As reported in Ref [51], with practical design, values for the amplification factor close to 10 can be achieved choosing the optimal frequency of modulation (~ 1 Hz). With these parameters used in the experimental setup [51], the modulation scheme presented here may lead to experimentally observable heat fluxes with higher amplitudes.

ACKNOWLEDGMENTS

N.G. and S.B. thank, respectively, CSIR (SRF) and DST INSPIRE for financial support through fellowships. A.G. is thankful for Initiation Grant, IITK (Grant No. IITK/CHM/2018513) and SRG (Grant No.

SRG/2019/000289), SERB, India for the partial financial support. B.D. is grateful to IACS for the fellowship. S.D. acknowledges the financial support from DST-SERB Grant No. ECR/2017/002037. S.D. also acknowledges support from the Technical Research Centre (TRC), IACS, Kolkata. V.M. acknowledges support from Science and Engineering Research Board (SERB) through MATRICS (Project No. MTR/2021/000055) and a Seed Grant from IISER Berhampur.

APPENDIX A: DERIVATION OF THE FLOQUET-MASTER EQUATION

We start with the interaction Hamiltonian

$$H_I = H_{IE} + H_{IB} + H_{IC} \\ = \sigma_x^E \otimes \mathcal{R}_E + \sigma_x^B \otimes \mathcal{R}_B + \sigma_x^C \otimes \mathcal{R}_C, \quad (\text{A1})$$

and in terms of the time-ordered unitary operator

$$U(t, 0) = \mathcal{T} \exp \left(-\frac{i}{\hbar} \int_0^t H_S(t') dt' \right), \quad (\text{A2})$$

we obtain the interaction picture von Neumann equation for the total density matrix $\rho_T(t)$ of the combined system as

$$\frac{d}{dt} \rho_T(t) = -\frac{i}{\hbar} [H_I(t), \rho_T(t)]. \quad (\text{A3})$$

Integrating the above equation and taking a trace over the bath degrees of freedom we obtain

$$\frac{d}{dt} \rho_s(t) = -\frac{1}{\hbar^2} \int_0^t ds \text{Tr}_{E,B,C} [H_I(t), [H_I(s), \rho_T(s)]], \quad (\text{A4})$$

where we use $\text{Tr}_{E,B,C} \{\rho_T(t)\} = \rho_s(t)$ and assume $\text{Tr}_{E,B,C} [H_I(t), \rho_T(0)] = 0$. Here $\text{Tr}_{E,B,C}$ refers to the trace over each bath degrees of freedom. Under the Born-Markov approximation, the reduced dynamics of the system in the weak system-bath coupling limit can be written as [25,41, 53–55]

$$\frac{d}{dt} \rho_s(t) = -\frac{1}{\hbar^2} \int_0^\infty ds \text{Tr}_{E,B,C} [H_I(t), [H_I(t-s), \rho_s(t) \otimes \rho_E \otimes \rho_B \otimes \rho_C]], \quad (\text{A5})$$

where we substitute $\rho_T(t) = \rho_s(t) \otimes \rho_E \otimes \rho_B \otimes \rho_C$. Here the interaction picture Hamiltonian [cf. Eq. (A1)] is given by

$$H_I(t) = \sum_{\alpha \in \{E,B,C\}} H_{I\alpha}(t), \\ H_{I\alpha}(t) = \sigma_x^\alpha(t) \otimes \mathcal{R}_\alpha(t) = (\sigma_+^\alpha(t) + \sigma_-^\alpha(t)) \\ \otimes \sum_k (g_k b_k^\alpha(t) + g_k^* b_k^{\alpha\dagger}(t)), \quad (\text{A6})$$

where $\mathcal{R}_\alpha(t) = \sum_k [g_k b_k^\alpha(t) + g_k^* b_k^{\alpha\dagger}(t)]$, satisfying $\langle \mathcal{R}_\alpha(t) \rangle = \text{Tr}_\alpha \{\mathcal{R}_\alpha(t) \rho_\alpha\} = 0$; $\alpha = E, B, C$. This implies [41,54,55]

$$\text{Tr}_{E,B,C} \{ [H_{I\alpha}(t), [H_{I\beta}(t-s), \rho_s(t) \otimes \rho_E \otimes \rho_B \otimes \rho_C]] \} \\ = 0; \quad \alpha \neq \beta, \quad \alpha, \beta = E, B, C. \quad (\text{A7})$$

As a result Eq. (A5) simplifies to

$$\frac{d}{dt}\rho_s(t) = -\frac{1}{\hbar^2} \sum_{\alpha \in \{B,C,E\}} \left\{ \int_0^\infty ds \text{Tr}_{E,B,C} \right. \\ \left. \times [H_{I\alpha}(t), [H_{I\alpha}(t-s), \rho_s(t) \otimes \rho_E \otimes \rho_B \otimes \rho_C]] \right\}. \quad (\text{A8})$$

Now deriving Eq. (3) from the above equation is straightforward, following the standard procedure for a single thermal reservoir [54] separately for each \mathcal{R}_α , while the calculation of system operator $\sigma_x^\alpha(t)$ requires some elucidations.

For the left (emitter) and right (collector) TLS system $\sigma_\pm(t)$ can be calculated in a straightforward way:

$$\sigma_\pm^\alpha(t) = U^\dagger(t, 0)\sigma_\pm^\alpha U(t, 0) = \exp\left[\frac{i}{\hbar} \int_0^t H_S(s) ds\right] \sigma_\pm^\alpha \\ \times \exp\left[-\frac{i}{\hbar} \int_0^t H_S(s) ds\right], \quad \alpha \in \{E, C\}, \quad (\text{A9})$$

where

$$H_S(t) = \frac{\hbar\omega_E}{2} \sigma_z^E + \frac{\hbar\omega_B(t)}{2} \sigma_z^B + \frac{\hbar\omega_C}{2} \sigma_z^C + \frac{\hbar\omega_{EB}}{2} \sigma_z^E \sigma_z^B \\ + \frac{\hbar\omega_{BC}}{2} \sigma_z^B \sigma_z^C + \frac{\hbar\omega_{CE}}{2} \sigma_z^C \sigma_z^E. \quad (\text{A10})$$

Among the six terms in the each exponent, only three terms will survive for each case; the time-dependent part of H_S also cancels from both sides of the exponent. Therefore, Eq. (A9) reduces to

$$\sigma_\pm^\alpha(t) = U^\dagger(t, 0)\sigma_\pm^\alpha U(t, 0) = \sum_{\{\Omega_\alpha\}} e^{\pm i\Omega_\alpha t} \sigma_\pm^\alpha, \quad \alpha \in \{E, C\}. \quad (\text{A11})$$

However, for the middle (base) TLS, the calculation of $\sigma_\pm^B(t)$ is nontrivial because of the presence of the time-dependent factor $\exp[i\omega_B(t)t]$ in $U(t, 0)$. However, our FQT system Hamiltonian is periodic in τ , $H_S(t + \tau) = H_S(t)$, so we use the Floquet theorem [40,41] to decompose the time evolution operator as $U(t, 0) = P(t)e^{Rt}$, where $P(t)$ is τ periodic and R is a constant operator. Because of the periodicity of $P(t)$, it follows from $U(0, 0) = \mathbb{1}$ that $P(0) = \mathbb{1}$ and hence $U(\tau, 0) = P(\tau)e^{R\tau} \equiv P(0)e^{R\tau} = e^{R\tau}$. We now identify the time-independent constant operator R with an effective Hamiltonian via

$$U(\tau, 0) = e^{R\tau} = e^{-\frac{i}{\hbar} \int_0^\tau H_S(t) dt} = e^{-iH_F\tau/\hbar}. \quad (\text{A12})$$

This effective Floquet Hamiltonian [an average over a full cycle of $H_S(t)$]

$$H_F = \frac{1}{\tau} \int_0^\tau H_S(t) dt \\ = \frac{\hbar\omega_E}{2} \sigma_z^E + \frac{\hbar\omega_0}{2} \sigma_z^B + \frac{\hbar\omega_C}{2} \sigma_z^C + \frac{\hbar\omega_{EB}}{2} \sigma_z^E \sigma_z^B \\ + \frac{\hbar\omega_{BC}}{2} \sigma_z^B \sigma_z^C + \frac{\hbar\omega_{CE}}{2} \sigma_z^C \sigma_z^E, \quad (\text{A13})$$

is defined by its quasienergy $\hbar\omega_j$ spectrum via the relation [10]

$$H_F = \sum_j \hbar\omega_j |j\rangle \langle j|; \quad j = 1, 2, \dots, 8. \quad (\text{A14})$$

Hence the part of the time-evolution operator can be decomposed as

$$e^{-iH_F t/\hbar} = \sum_j e^{-i\omega_j t} |j\rangle \langle j|; \quad j = 1, 2, \dots, 8. \quad (\text{A15})$$

Likewise the expansion of the periodic function $P(t)$ reads [41]

$$P(t) = \sum_{q \in \mathbb{Z}} \tilde{P}(q) e^{-iqvt}; \quad \tilde{P}(q) = \frac{1}{\tau} \int_0^\tau P(t, 0) e^{iqvt} dt, \quad (\text{A16})$$

which results in the time-evolution operator as

$$U(t, 0) = \sum_{q \in \mathbb{Z}} \sum_j \tilde{P}(q) e^{-iqvt} e^{-i\omega_j t} |j\rangle \langle j|; \quad j = 1, 2, \dots, 8. \quad (\text{A17})$$

Thus, the system operator $\sigma_\pm^B(t)$ is then given by in interaction picture as [41,56]

$$\sigma_x^B(t) = U^\dagger(t, 0)\sigma_x^B U(t, 0) \\ = \sum_{q \in \mathbb{Z}} \sum_{\{\Omega_B\}} (\xi(q) e^{-i(\Omega_B + qv)t} \sigma_- + \bar{\xi}(q) e^{i(\Omega_B + qv)t} \sigma_+), \quad (\text{A18})$$

where

$$\xi(q) = \frac{1}{\tau} \int_0^\tau \exp\left(-i \int_0^t [\omega_B(s) - \omega_0] ds\right) e^{iqvt} dt. \quad (\text{A19})$$

Here $\nu = 2\pi/\tau$, q are integers and $\{\Omega_\alpha\}$ corresponds to the set of all transition frequencies where $\omega_{ij} = \omega_i - \omega_j > 0$ are the possible excitation energies between the levels of H_F . It is evident due to the absence of any modulation for the emitter and collector terminals that we will obtain the same expressions for $\sigma_\pm^{E(C)}(t)$ whether we use Eq. (A13) or Eq. (A10) in Eq. (A9) for $U(t, 0)$. In what follows, we therefore write down the master equation and derive its steady state solution in terms of the time-averaged Floquet Hamiltonian since our overall system Hamiltonian is time periodic.

With the help of Eqs. (A9) and (A18) and averaging out over the rapidly oscillating terms in Eq. (A8) within secular approximation, we arrive at the reduced master equation in the interaction picture [6,41–43,45,48,53–57]

$$\dot{\rho}_s(t) = \mathcal{L}_E[\rho_s] + \tilde{\mathcal{L}}_B[\rho_s] + \mathcal{L}_C[\rho_s], \\ \tilde{\mathcal{L}}_B[\rho_s] = \sum_{q \in \mathbb{Z}} \sum_{\{\Omega_B\}} \mathcal{L}_{q\Omega_B}^B[\rho_s], \quad \mathcal{L}_{E(C)}[\rho_s] = \sum_{\{\Omega_{E(C)}\}} \mathcal{L}_{\Omega_{E(C)}}^{E(C)}[\rho_s]. \quad (\text{A20})$$

where

$$\begin{aligned}\mathcal{L}_{\Omega_{E(C)}}^{E(C)}[\rho_s] &= G_{E(C)}(\Omega_{E(C)})(\sigma_- \rho_s(t) \sigma_+ - \frac{1}{2}\{\sigma_+ \sigma_-, \rho_s(t)\}) + G_{E(C)}(-\Omega_{E(C)})(\sigma_+ \rho_s(t) \sigma_- - \frac{1}{2}\{\sigma_- \sigma_+, \rho_s(t)\}); \\ \mathcal{L}_{q\Omega_B}^B[\rho_s] &= P_q[G_B(\Omega_B + q\nu)(\sigma_- \rho_s(t) \sigma_+ - \frac{1}{2}\{\sigma_+ \sigma_-, \rho_s(t)\}) + G_B(-\Omega_B - q\nu)(\sigma_+ \rho_s(t) \sigma_- - \frac{1}{2}\{\sigma_- \sigma_+, \rho_s(t)\})]\end{aligned}\quad (\text{A21})$$

and P_q is the q th harmonic weights that are calculated as $P_q = |\xi(q)|^2 = P_{-q}$. Here we define the temperature-dependent bath response spectra or autocorrelation function sampled as

$$\begin{aligned}G_B[(\Omega_B + q\nu)] &:= \int_{-\infty}^{\infty} e^{i(\Omega_B + q\nu)t} \langle \mathcal{R}_\alpha(t) \mathcal{R}_\alpha(0) \rangle dt, \\ G_{E(C)}[\Omega_{E(C)}] &:= \int_{-\infty}^{\infty} e^{i\Omega_{E(C)}t} \langle \mathcal{R}_\alpha(t) \mathcal{R}_\alpha(0) \rangle dt,\end{aligned}\quad (\text{A22})$$

where $\mathcal{R}_\alpha(t) = e^{iH_R t} \mathcal{R}_\alpha e^{-iH_R t}$, $\alpha \in \{E, B, C\}$. Which fulfills the detailed-balance Kubo-Martin-Schwinger (KMS) condition $G_\alpha(-\Omega) = e^{-\beta_\alpha \hbar \Omega} G_\alpha(\Omega)$ [54]. Equation (A21) stands for Eq. (4) in the main text.

APPENDIX B: DERIVATION OF STEADY STATE HEAT CURRENT

Eight equations given by Eq. (6) are not independent since $\text{Tr} \rho = 1$. This uniquely solves all state occupation probabilities as well as the currents. To determine the heat currents we first note that the master Eq. (A20) drives the system to a Gibbs-like stationary state. As stated in the previous section, since the overall system is time periodic, stationary state solutions of the master Eq. (A21) can be expressed in the form of the average Floquet Hamiltonian [6]

$$\begin{aligned}\rho_{B,ss}^{q,\Omega} &= \mathcal{Z}_B^{-1} \exp\left(-\frac{\Omega_B + q\nu}{\Omega_B} \beta_B H_F\right), \\ \rho_{\alpha,ss} &= \mathcal{Z}_\alpha^{-1} \exp(-\beta_\alpha H_F), \quad \alpha \in \{E, C\},\end{aligned}\quad (\text{B1})$$

where $\mathcal{Z}_B = \text{Tr}[\exp(-\frac{\Omega_B + q\nu}{\Omega_B} \beta_B H_F)]$ and $\mathcal{Z}_\alpha = \text{Tr}[\exp(-\beta_\alpha H_F)]$. Then the thermal current or heat flow is defined by making use of the dynamical version of the second law in terms of von Neumann entropy [6]. Upon taking the time derivative of the von Neumann entropy $S[\rho_s(t)] = -k_B \text{Tr}[\rho_s(t) \ln \rho_s(t)]$, we obtains

$$\begin{aligned}\frac{d}{dt} S[\rho_s(t)] &= -k_B \sum_{\alpha \in \{E, C\}} \sum_{\{\Omega\}} \text{Tr}[\mathcal{L}_{\Omega}^\alpha \rho_s(t) \ln \rho_s(t)] \\ &\quad - k_B \sum_{q \in \mathbb{Z}} \sum_{\{\Omega\}} \text{Tr}[\mathcal{L}_{q\Omega}^B \rho_s(t) \ln \rho_s(t)],\end{aligned}\quad (\text{B2})$$

where we used Eq. (4) and $\text{Tr}[\dot{\rho}] = 0$. Now, with the help of the Spohn inequality [46] and dynamical version of the second law of thermodynamics [43], we can write down the simplified version of the steady state thermal current as

$$J_B^{ss} = \sum_{q \in \mathbb{Z}} \sum_{\Omega_B} \frac{\Omega_B + q\nu}{\Omega_B} \text{Tr}[(\mathcal{L}_{q\Omega_B}^B[\rho^{ss}]) H_F], \quad (\text{B3})$$

$$J_\alpha^{ss} = \sum_{\Omega_\alpha} \text{Tr}[\mathcal{L}_{\Omega_\alpha}^\alpha[\rho^{ss}] H_F], \quad \alpha \in \{E, C\}. \quad (\text{B4})$$

Since only the base terminal is periodically modulated, only J_B contains the direct signature of the modulation, while $J_{E(C)}$ does not.

Dropping the superscript and carrying out the trace over the system states, we derive the explicit expressions for the steady state heat currents using Eq. (B1), (B3), and (B4).

$$J_{E(C)} = -\hbar \sum_{\omega_{ij}} \omega_{ij} \Gamma_{ij}^{E(C)}, \quad (\text{B5})$$

$$J_B = -\hbar \sum_q \sum_{\omega_{ij}} (\omega_{ij} + q\nu) \Gamma_{ij,q}^B, \quad (\text{B6})$$

where the net decaying rates are as follows:

$$\begin{aligned}\Gamma_{ij}^{E(C)} &= [G_{E(C)}(\omega_{ij}) \rho_{ii}^{ss} - G_{E(C)}(-\omega_{ij}) \rho_{jj}^{ss}], \\ \Gamma_{ij,q}^B &= P_q [G_B(\omega_{ij} + q\nu) \rho_{ii}^{ss} - G_B(-\omega_{ij} - q\nu) \rho_{jj}^{ss}].\end{aligned}\quad (\text{B7})$$

APPENDIX C: COMMON BASE TRANSISTOR

We now derive approximate expressions for the levels populations, thermal currents, decay rates, and analyze the conditions required for the satisfaction of the Born-Markov approximation. We finally discuss the conditions needed for observing the thermal transistor effect. To reduce the number of the states, we set the bare frequencies of all the TLSs as zero and the two nonzero couplings as symmetric

$$\begin{aligned}\omega_E = 0, \quad \omega_0 = 0, \quad \omega_C = 0, \quad \omega_{EB} = \Delta, \\ \omega_{BC} = \Delta > 0.\end{aligned}\quad (\text{C1})$$

As shown in the main text, in these conditions, the system states are degenerate two by two, viz. $|1\rangle = |8\rangle \equiv |I\rangle$, $|2\rangle = |7\rangle \equiv |II\rangle$, $|3\rangle = |6\rangle \equiv |III\rangle$, and $|4\rangle = |5\rangle \equiv |IV\rangle$. Moreover, there are only three energy levels: $E_1 = E_8 = \Delta$, $E_2 = E_4 = E_5 = E_7 = 0$, and $E_3 = E_6 = -\Delta$ (Fig. 2 of the main text). Further, we introduce new density matrix elements, now reduced to four, $\rho_I = \rho_{11} + \rho_{88}$, $\rho_{II} = \rho_{22} + \rho_{77}$, $\rho_{III} = \rho_{33} + \rho_{66}$, and $\rho_{IV} = \rho_{44} + \rho_{55}$. We also define the net decaying rate with respect to these new density matrix elements in the same manner. Now we modulate the bare frequency of the base TLS in such a manner that we fix $\omega_0 = 0$, i.e., the average over a time period is set to zero. Hence, on an average over the time period, the energy of the newly defined states remains the same as that considered in Ref. [22]. It is worthwhile to mention that the average effective Floquet Hamiltonian is essentially the same as the time-independent Hamiltonian of Ref. [22]. In the same spirit, for this choice of parameter, we can analyze the system to obtain the following time-evolution of the new density-matrix:

$$\begin{aligned}\dot{\rho}_I &= \Gamma_{IV-I}^E + \Gamma_{III-I}^B + \Gamma_{II-I}^C, \\ \dot{\rho}_{II} &= \Gamma_{III-II}^E + \Gamma_{IV-II}^B + \Gamma_{I-II}^C,\end{aligned}$$

$$\begin{aligned}\dot{\rho}_{III} &= \Gamma_{II-III}^E + \Gamma_{I-III}^B + \Gamma_{IV-III}^C, \\ \dot{\rho}_{IV} &= \Gamma_{I-IV}^E + \Gamma_{II-IV}^B + \Gamma_{III-IV}^C.\end{aligned}\quad (\text{C2})$$

For our problem of interest we consider $\{T_E, T_B, T_C\} \ll \hbar\Delta/k_B$, hence $e^{\hbar\Delta/k_B T_a} \gg 1$, which allows us to simplify the expressions of the decay rates. Finally, we obtain

$$\begin{aligned}\Gamma_{I-IV}^E &= \kappa\Delta\{\rho_I - e^{-\hbar\Delta/k_B T_E}\rho_{IV}\}, \\ \Gamma_{II-III}^E &= \kappa\Delta\{\rho_{II} - e^{-\hbar\Delta/k_B T_E}\rho_{III}\}, \\ \Gamma_{IV-III}^C &= \kappa\Delta\{\rho_{IV} - e^{-\hbar\Delta/k_B T_C}\rho_{III}\}, \\ \Gamma_{I-II}^C &= \kappa\Delta\{\rho_I - e^{-\hbar\Delta/k_B T_C}\rho_{II}\}.\end{aligned}\quad (\text{C3})$$

Here we point out that $\Gamma_{ij} = -\Gamma_{ji}$. In a similar manner, considering up to the first two harmonics, we can approximate the

decay rates induced by the base terminal

$$\begin{aligned}\Gamma_{I-III}^B &= \kappa \sum_{q=0,\pm 1} P_q(2\Delta + qv)\{\rho_I - e^{-\hbar(2\Delta+qv)/k_B T_B}\rho_{III}\}, \\ \Gamma_{IV-II}^B &= P_0(k_B T_B/\hbar)[\rho_{IV} - \rho_{II}] \\ &\quad + P_1 v(2\bar{n}_B(v) + 1)[\rho_{IV} - \rho_{II}].\end{aligned}\quad (\text{C4})$$

Next, we would set the Eq. (C2) equal to zero and solve the system of linear equations to obtain the steady state solutions of the density matrix elements, subject to the condition

$$\text{Tr}[\rho] = \rho_I + \rho_{II} + \rho_{III} + \rho_{IV} = 1. \quad (\text{C5})$$

The set of equations can be rewritten in the form

$$[M] \begin{bmatrix} \rho_I \\ \rho_{II} \\ \rho_{III} \\ \rho_{IV} \end{bmatrix} = \begin{bmatrix} 0 \\ 0 \\ 0 \\ 1 \end{bmatrix}, \quad (\text{C6})$$

with

$$M = \begin{bmatrix} -2\Delta(1 + P_0 + 2P_1) & \Delta e^{-\hbar\Delta/k_B T_C} & 2F(v)\Delta & \Delta e^{-\hbar\Delta/k_B T_E} \\ \Delta & -(\Delta + P_0 k_B T_B/\hbar + P_1 v N(v) + \Delta e^{-\hbar\Delta/k_B T_C}) & \Delta e^{-\hbar\Delta/k_B T_E} & P_0 k_B T_B/\hbar + P_1 v N(v) \\ 2\Delta(P_0 + 2P_1) & \Delta & \Delta(e^{-\hbar\Delta/k_B T_E} + 2F(v) + e^{-\hbar\Delta/k_B T_C}) & \Delta \\ 1 & 1 & 1 & 1 \end{bmatrix}, \quad (\text{C7})$$

where

$$\begin{aligned}F(v) &= \exp(-2\hbar\Delta/k_B T_B) \left[P_0 + P_1 \left(1 + \frac{v}{2\Delta} \right) \exp(-\hbar v/k_B T_B) + P_1 \left(1 - \frac{v}{2\Delta} \right) \exp(\hbar v/k_B T_B) \right], \\ N(v) &= \frac{1}{e^{\hbar v/k_B T_B} - 1} - \frac{1}{e^{-\hbar v/k_B T_B} - 1} = 2\bar{n}_B^B + 1.\end{aligned}\quad (\text{C8})$$

Under the condition of the system parameters $\{T_E, T_B, T_C\} \ll \hbar\Delta/k_B$, we can simplify the matrix M following $e^{-\hbar\Delta/k_B T_a} \ll 1$, as

$$M \approx \begin{bmatrix} 2\Delta(1 + P_0 + 2P_1) & 0 & 0 & -\Delta e^{-\hbar\Delta/k_B T_E} \\ \Delta & -\Delta - (P_0 k_B T_B/\hbar) - P_1 v N(v) & \Delta e^{-\hbar\Delta/k_B T_E} & (P_0 k_B T_B/\hbar) + P_1 v N(v) \\ 2\Delta(P_0 + 2P_1) & \Delta & -\Delta e^{-\hbar\Delta/k_B T_E} & \Delta \\ 1 & 1 & 1 & 1 \end{bmatrix}. \quad (\text{C9})$$

Now, from this simplified matrix Eq. (C9), the matrix determinant can also be simplified

$$\begin{aligned}\det[M] &\simeq 2\Delta^2(1 + P_0 + 2P_1) \left[\Delta + 2P_0 \left(\frac{k_B T_B}{\hbar} \right) + 2P_1 v \left(\frac{e^{\hbar v/k_B T_B} + 1}{e^{\hbar v/k_B T_B} - 1} \right) \right] (1 + e^{-\hbar\Delta/k_B T_E}) \\ &\quad + \Delta^2 \left[\Delta + 2P_0 \left(\frac{k_B T_B}{\hbar} \right) (P_0 + 2P_1) + 2P_1 v \left(\frac{e^{\hbar v/k_B T_B} + 1}{e^{\hbar v/k_B T_B} - 1} \right) (P_0 + 2P_1) \right] e^{-\hbar\Delta/k_B T_E} \\ &\simeq 2\Delta^2(1 + P_0 + 2P_1) \left[\Delta + 2P_0 \left(\frac{k_B T_B}{\hbar} \right) + 2P_1 v \left(\frac{e^{\hbar v/k_B T_B} + 1}{e^{\hbar v/k_B T_B} - 1} \right) \right] \\ &\quad + \Delta^2 \left[\Delta(3 + 4P_0 + 8P_1) + 2P_0 \left(\frac{k_B T_B}{\hbar} \right) (2 + 3P_0 + 6P_1) + 2P_1 v \left(\frac{e^{\hbar v/k_B T_B} + 1}{e^{\hbar v/k_B T_B} - 1} \right) (2 + 3P_0 + 6P_1) \right] e^{-\hbar\Delta/k_B T_E} \\ &\approx 2\Delta^2(1 + P_0 + 2P_1) \left[\Delta + 2P_0 \left(\frac{k_B T_B}{\hbar} \right) + 2P_1 v \left(\frac{e^{\hbar v/k_B T_B} + 1}{e^{\hbar v/k_B T_B} - 1} \right) \right],\end{aligned}\quad (\text{C10})$$

so that the right-hand side (r.h.s.) of Eq. (C10), and therefore the populations' expressions, become independent of the collector temperature T_C . With Eq. (C9), the evaluation of the approximated population expressions becomes straightforward:

$$\rho_I \simeq \frac{1}{2(1 + P_0 + 2P_1)} \frac{(P_0 k_B T_B/\hbar) + P_1 v \left(\frac{e^{\hbar v/k_B T_B} + 1}{e^{\hbar v/k_B T_B} - 1} \right)}{(2P_0 k_B T_B/\hbar) + 2P_1 v \left(\frac{e^{\hbar v/k_B T_B} + 1}{e^{\hbar v/k_B T_B} - 1} \right) + \Delta} e^{-2\hbar\Delta/k_B T_E}, \quad (\text{C11})$$

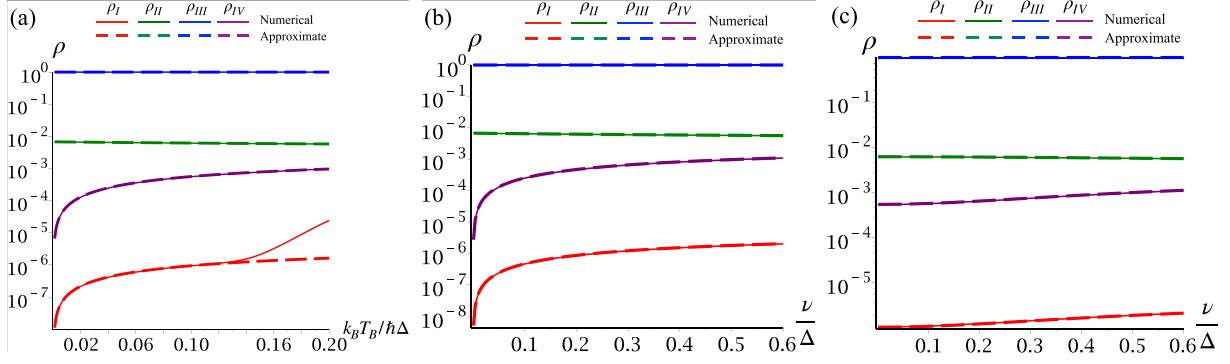


FIG. 9. Populations ρ_I , ρ_{II} , ρ_{III} , and ρ_{IV} as a function of (a) $k_B T_B / \hbar \Delta$ for the unmodulated case, (b) as a function of ν / Δ for π modulation in the limit $T_B \rightarrow 0$, and (c) as a function of ν / Δ for π modulation, for $k_B T_B = 0.118 \hbar \Delta$. Here we take $\omega_E = \omega_0 = \omega_C = 0$, $\omega_{CE} = 0$, $\omega_{EB} = \omega_{BC} = \Delta$, $k_B T_E = 0.2 \hbar \Delta$, and $k_B T_C = 0.02 \hbar \Delta$. As seen above, numerical results match the analytical ones as long as T_B is not large.

$$\rho_{II} \simeq \frac{(P_0 k_B T_B / \hbar) + P_1 \nu \left(\frac{e^{\hbar \nu / k_B T_B} + 1}{e^{\hbar \nu / k_B T_B} - 1} \right) + \Delta}{(2P_0 k_B T_B / \hbar) + 2P_1 \nu \left(\frac{e^{\hbar \nu / k_B T_B} + 1}{e^{\hbar \nu / k_B T_B} - 1} \right) + \Delta} e^{-\hbar \Delta / k_B T_E}, \quad (\text{C12})$$

$$\rho_{III} \simeq 1 - e^{-\hbar \Delta / k_B T_E}, \quad (\text{C13})$$

$$\rho_{IV} \simeq \frac{(P_0 k_B T_B / \hbar) + P_1 \nu \left(\frac{e^{\hbar \nu / k_B T_B} + 1}{e^{\hbar \nu / k_B T_B} - 1} \right)}{(2P_0 k_B T_B / \hbar) + 2P_1 \nu \left(\frac{e^{\hbar \nu / k_B T_B} + 1}{e^{\hbar \nu / k_B T_B} - 1} \right) + \Delta} e^{-\hbar \Delta / k_B T_E}. \quad (\text{C14})$$

In Figs. 9 and 10, we show the comparison between the population values calculated by their exact expressions with the analytical ones. Similarly, we obtain the approximate decaying rates in Eq. (C15)

$$\Gamma_{I-IV}^E = -\kappa \Delta \left(\frac{1 + 2P_0 + 4P_1}{2(1 + P_0 + 2P_1)} \right) \frac{P_0 k_B T_B + P_1 \hbar \nu \left(\frac{e^{\hbar \nu / k_B T_B} + 1}{e^{\hbar \nu / k_B T_B} - 1} \right)}{2P_0 k_B T_B + 2P_1 \hbar \nu \left(\frac{e^{\hbar \nu / k_B T_B} + 1}{e^{\hbar \nu / k_B T_B} - 1} \right) + \hbar \Delta} e^{-2\hbar \Delta / k_B T_E},$$

$$\Gamma_{II-III}^E = -\kappa \Delta \frac{P_0 k_B T_B + P_1 \hbar \nu \left(\frac{e^{\hbar \nu / k_B T_B} + 1}{e^{\hbar \nu / k_B T_B} - 1} \right)}{2P_0 k_B T_B + 2P_1 \hbar \nu \left(\frac{e^{\hbar \nu / k_B T_B} + 1}{e^{\hbar \nu / k_B T_B} - 1} \right) + \hbar \Delta} e^{-\hbar \Delta / k_B T_E},$$

$$\Gamma_{IV-III}^C = \kappa \Delta \frac{P_0 k_B T_B + P_1 \hbar \nu \left(\frac{e^{\hbar \nu / k_B T_B} + 1}{e^{\hbar \nu / k_B T_B} - 1} \right)}{2P_0 k_B T_B + 2P_1 \hbar \nu \left(\frac{e^{\hbar \nu / k_B T_B} + 1}{e^{\hbar \nu / k_B T_B} - 1} \right) + \hbar \Delta} e^{-\hbar \Delta / k_B T_E},$$

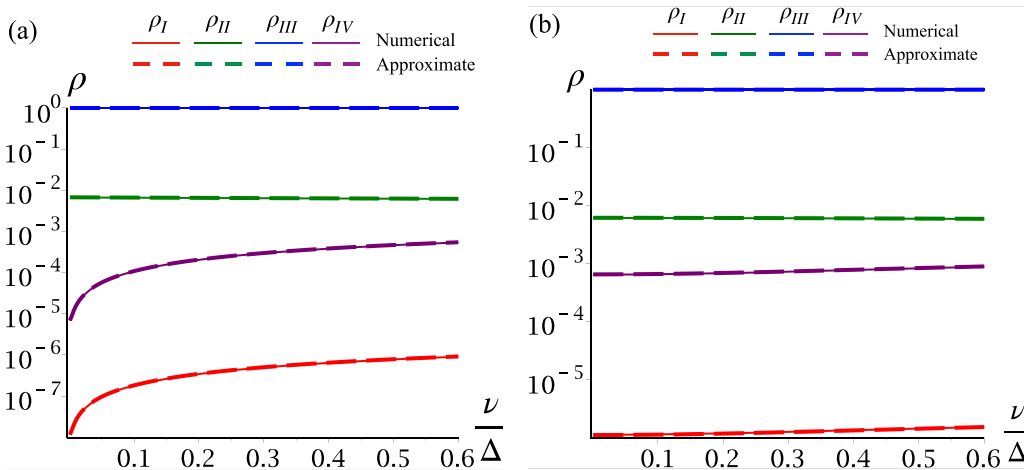


FIG. 10. Populations ρ_I , ρ_{II} , ρ_{III} , and ρ_{IV} versus ν / Δ under sinusoidal modulation with the parameters $\omega_E = \omega_0 = \omega_C = 0$, $\omega_{CE} = 0$, $\omega_{EB} = \omega_{BC} = \Delta$, $k_B T_E = 0.2 \hbar \Delta$, and $k_B T_C = 0.02 \hbar \Delta$. (a) For generic case when $T_B \rightarrow 0$ and (b) $k_B T_B = 0.118 \hbar \Delta$. Comparison is done between populations obtained from the exact numerical calculations and the approximated analytical expressions derived here.

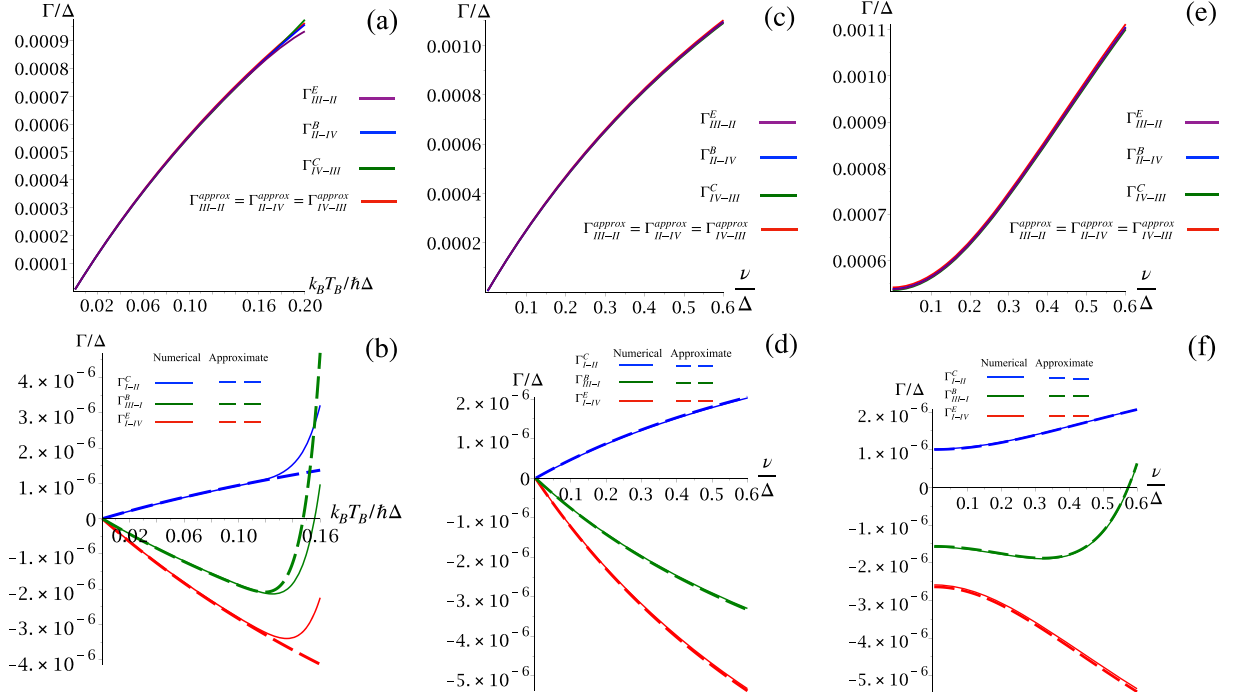


FIG. 11. Decaying rates Γ_{III-II}^E , Γ_{II-IV}^B , Γ_{IV-III}^C , and Γ_{I-IV}^E , Γ_{III-II}^B , Γ_{II-IV}^E as a function of (a,b) $k_B T_B / \hbar \Delta$ for the unmodulated case, (c,d) as a function of ν / Δ in presence of π -modulation, for $T_B \rightarrow 0$, (e,f) as a function of ν / Δ in presence of π -modulation case for $k_B T_B = 0.118 \hbar \Delta$, respectively. Here we take $\omega_E = \omega_0 = \omega_C = 0$, $\omega_{CE} = 0$, $\omega_{EB} = \omega_{BC} = \Delta$, $k_B T_E = 0.2 \hbar \Delta$, and $k_B T_C = 0.02 \hbar \Delta$. Analytical results match the numerical ones, except for large T_B .

$$\begin{aligned}
 \Gamma_{I-II}^C &\simeq \kappa \Delta \frac{1}{2(1+P_0+2P_1)} \frac{P_0 k_B T_B + P_1 \hbar \nu \left(\frac{e^{\hbar \nu / k_B T_B} + 1}{e^{\hbar \nu / k_B T_B} - 1} \right)}{2P_0 k_B T_B + 2P_1 \hbar \nu \left(\frac{e^{\hbar \nu / k_B T_B} + 1}{e^{\hbar \nu / k_B T_B} - 1} \right) + \hbar \Delta} e^{-2\hbar \Delta / k_B T_E}, \\
 \Gamma_{I-III,q}^B &= \kappa \sum_{q=0,\pm 1} P_q (2\Delta + q\nu) \left[\frac{1}{2(1+P_0+2P_1)} \left(\frac{P_0 k_B T_B + P_1 \hbar \nu \left(\frac{e^{\hbar \nu / k_B T_B} + 1}{e^{\hbar \nu / k_B T_B} - 1} \right)}{2P_0 k_B T_B + 2P_1 \hbar \nu \left(\frac{e^{\hbar \nu / k_B T_B} + 1}{e^{\hbar \nu / k_B T_B} - 1} \right) + \hbar \Delta} \right) e^{-2\hbar \Delta / k_B T_E} - e^{-\hbar(2\Delta + q\nu) / k_B T_B} \right], \\
 \Gamma_{IV-II,q}^B &= -\kappa \Delta \frac{P_0 k_B T_B + P_1 \hbar \nu \left(\frac{e^{\hbar \nu / k_B T_B} + 1}{e^{\hbar \nu / k_B T_B} - 1} \right)}{2P_0 k_B T_B + 2P_1 \hbar \nu \left(\frac{e^{\hbar \nu / k_B T_B} + 1}{e^{\hbar \nu / k_B T_B} - 1} \right) + \hbar \Delta} e^{-\hbar \Delta / k_B T_E}. \tag{C15}
 \end{aligned}$$

An important point to note in Fig. 11 is that the scaled decaying rates are $\sim 10^{-6}$ – 10^{-7} , which are much smaller than 1. Also from Fig. 12 we can see that the case of sinusoidal modulation where the decaying rates' values have the same order as in the case of π -flip modulation.

This implies that the system relaxation time ($1/\Gamma$) is much longer than the timescale associated with the inverse of the frequency difference ($\sim 1/\Delta$) involved in the problem, thereby justifying the Born-Markov approximation in this regime. On the other hand, larger Γ at higher T_B may invalidate the Born-Markov approximation [see Eq. (C3)]. Therefore, we confine ourselves to low temperatures and modulate the base frequency to illustrate the transistor effect.

Finally, we calculate the approximate form of the steady state thermal currents

$$J_E \simeq \kappa \hbar \Delta^2 \left[\frac{P_0 k_B T_B + P_1 \hbar \nu \left(\frac{e^{\hbar \nu / k_B T_B} + 1}{e^{\hbar \nu / k_B T_B} - 1} \right)}{2P_0 k_B T_B + 2P_1 \hbar \nu \left(\frac{e^{\hbar \nu / k_B T_B} + 1}{e^{\hbar \nu / k_B T_B} - 1} \right) + \hbar \Delta} \right] e^{-\hbar \Delta / k_B T_E}, \tag{C16}$$

$$J_B = \kappa \sum_{q=0,\pm 1} P_q \hbar (2\Delta + q\nu)^2 \left[e^{-\hbar(2\Delta + q\nu) / k_B T_B} - \frac{1}{2(1+P_0+2P_1)} \left(\frac{P_0 k_B T_B + P_1 \hbar \nu \left(\frac{e^{\hbar \nu / k_B T_B} + 1}{e^{\hbar \nu / k_B T_B} - 1} \right)}{2P_0 k_B T_B + 2P_1 \hbar \nu \left(\frac{e^{\hbar \nu / k_B T_B} + 1}{e^{\hbar \nu / k_B T_B} - 1} \right) + \hbar \Delta} \right) e^{-2\hbar \Delta / k_B T_E} \right],$$

$$J_C \simeq -\kappa \hbar \Delta^2 \left[\frac{P_0 k_B T_B + P_1 \hbar \nu \left(\frac{e^{\hbar \nu / k_B T_B} + 1}{e^{\hbar \nu / k_B T_B} - 1} \right)}{2P_0 k_B T_B + 2P_1 \hbar \nu \left(\frac{e^{\hbar \nu / k_B T_B} + 1}{e^{\hbar \nu / k_B T_B} - 1} \right) + \hbar \Delta} \right] e^{-\hbar \Delta / k_B T_E}. \tag{C17}$$

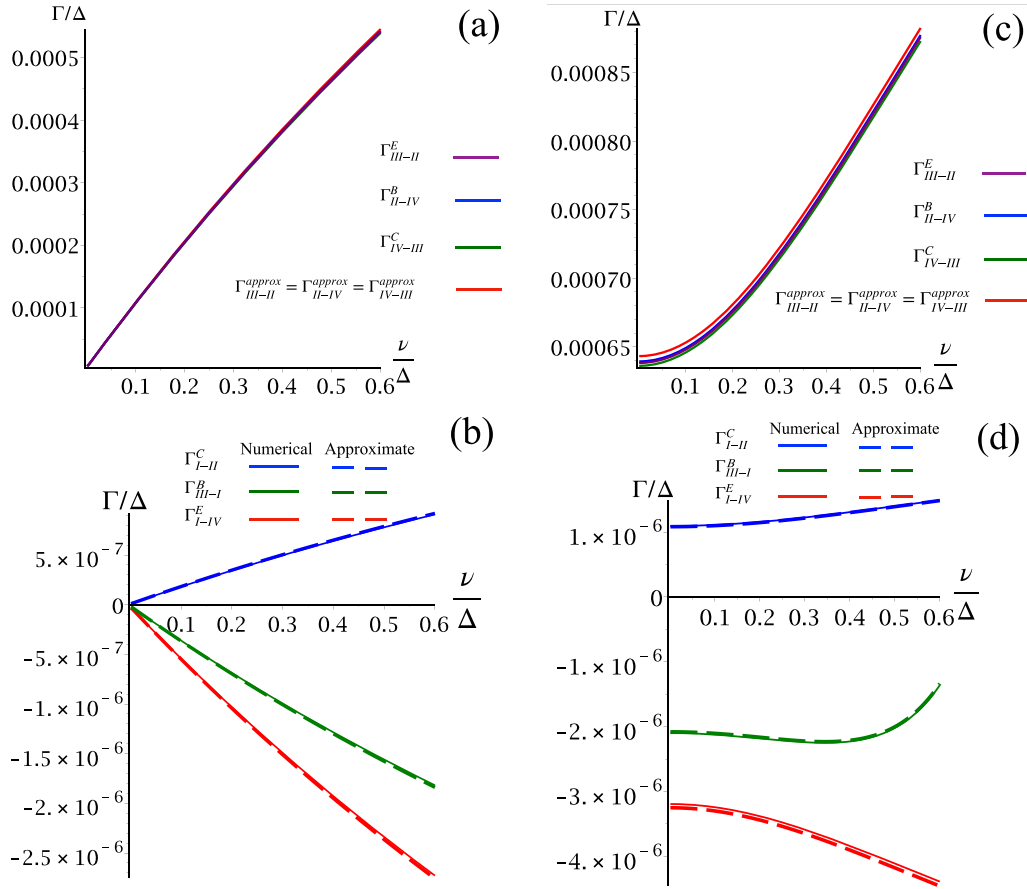


FIG. 12. Decaying rates Γ_{III-II}^E , Γ_{II-IV}^B , Γ_{IV-III}^C and Γ_{I-II}^C , Γ_{II-I}^B , Γ_{I-IV}^E as a function ν/Δ in presence of sinusoidal modulation, for (a) and (b) $T_B \rightarrow 0$, and (c) and (d) for $k_B T_B = 0.118\hbar\Delta$. Here we take $\omega_E = \omega_0 = \omega_C = 0$, $\omega_{CE} = 0$, $\omega_{EB} = \omega_{BC} = \Delta$, $k_B T_E = 0.2\hbar\Delta$, $k_B T_C = 0.02\hbar\Delta$. Comparison is done between decay rates obtained from the exact numerical calculations and the approximated analytical expressions.

- [1] J. Millen and A. Xuereb, *Phys. World* **29**, 23 (2016).
- [2] V. Mukherjee and U. Divakaran, *J. Phys.: Condens. Matter* **33**, 454001 (2021).
- [3] N. M. Myers, O. Abah, and S. Deffner, *AVS Quantum Sci.* **4**, 027101 (2022).
- [4] A. Ghosh, V. Mukherjee, W. Niedenzu, and G. Kurizki, *Eur. Phys. J.: Spec. Top.* **227**, 2043 (2019).
- [5] S. Deffner and S. Campbell, *Quantum Thermodynamics: An Introduction to the Thermodynamics of Quantum Information* (Morgan and Claypool, Williston, VT, 2019).
- [6] D. Gelbwaser-Klimovsky, W. Niedenzu, and G. Kurizki, *Adv. At. Mol. Opt. Phys.* **64**, 329 (2015).
- [7] A. Ghosh, D. Gelbwaser-Klimovsky, W. Niedenzu, A. I. Lvovsky, I. Mazets, M. O. Scully, and G. Kurizki, *Proc. Natl. Acad. Sci.* **115**, 9941 (2018).
- [8] S. Vinjanampathy and J. Anders, *Contemp. Phys.* **57**, 545 (2016).
- [9] F. Binder, L. Correa, C. Gogolin, J. Anders, and G. Adesso, *Thermodynamics in the Quantum Regime: Fundamental Aspects and New Directions*, Fundamental Theories of Physics (Springer International Publishing, New York, 2019).
- [10] S. Bhattacharjee and A. Dutta, *Eur. Phys. J. B* **94**, 239 (2021).
- [11] N. Gupta, S. Bhattacharyya, and A. Ghosh, *Phys. Rev. E* **104**, 054130 (2021).
- [12] G. Kurizki, P. Bertet, Y. Kubo, K. Moelmer, D. Petrosyan, P. Rabl, and J. Schmiedmayer, *Proc. Natl. Acad. Sci. USA* **112**, 3866 (2015).
- [13] A. Ghosh, C. L. Latune, L. Davidovich, and G. Kurizki, *Proc. Natl. Acad. Sci.* **114**, 12156 (2017).
- [14] S. Rosi, A. Bernard, N. Fabbri, L. Fallani, C. Fort, M. Inguscio, T. Calarco, and S. Montangero, *Phys. Rev. A* **88**, 021601(R) (2013).
- [15] F. Borselli, M. Maiwöger, T. Zhang, P. Haslinger, V. Mukherjee, A. Negretti, S. Montangero, T. Calarco, I. Mazets, M. Bonneau, and J. Schmiedmayer, *Phys. Rev. Lett.* **126**, 083603 (2021).
- [16] J. Roßnagel, S. T. Dawkins, K. N. Tolazzi, O. Abah, E. Lutz, F. Schmidt-Kaler, and K. Singer, *Science* **352**, 325 (2016).
- [17] J. Klaers, S. Faelt, A. Imamoglu, and E. Togan, *Phys. Rev. X* **7**, 031044 (2017).
- [18] J. Klatzow, J. N. Becker, P. M. Ledingham, C. Weinzetl, K. T. Kaczmarek, D. J. Saunders, J. Nunn, I. A. Walmsley, R. Uzdin, and E. Poem, *Phys. Rev. Lett.* **122**, 110601 (2019).
- [19] G. Maslennikov, S. Ding, R. Häblützel, J. Gan, A. Roulet, S. Nimmrichter, J. Dai, V. Scarani, and D. Matsukevich, *Nat. Commun.* **10**, 202 (2019).

- [20] V. Lashkaryov, *Izv. Akad. Nauk SSSR, Ser. Fiz* **5**, 442 (1941).
- [21] J.-H. Jiang, M. Kulkarni, D. Segal, and Y. Imry, *Phys. Rev. B* **92**, 045309 (2015).
- [22] K. Joulain, J. Drevillon, Y. Ezzahri, and J. Ordonez-Miranda, *Phys. Rev. Lett.* **116**, 200601 (2016).
- [23] M. Majland, K. S. Christensen, and N. T. Zinner, *Phys. Rev. B* **101**, 184510 (2020).
- [24] A. Mandarin, K. Joulain, M. D. Gómez, and B. Bellomo, *Phys. Rev. Applied* **16**, 034026 (2021).
- [25] R. T. Wijesekara, S. D. Gunapala, and M. Premaratne, *Phys. Rev. B* **104**, 045405 (2021).
- [26] W. C. Lo, L. Wang, and B. Li, *J. Phys. Soc. Jpn.* **77**, 054402 (2008).
- [27] B. Li, L. Wang, and G. Casati, *Appl. Phys. Lett.* **88**, 143501 (2006).
- [28] O.-P. Saira, M. Meschke, F. Giazotto, A. M. Savin, M. Möttönen, and J. P. Pekola, *Phys. Rev. Lett.* **99**, 027203 (2007).
- [29] H. Prod'homme, J. Ordonez-Miranda, Y. Ezzahri, J. Drevillon, and K. Joulain, *J. Appl. Phys.* **119**, 194502 (2016).
- [30] J. Ordonez-Miranda, Y. Ezzahri, J. Drevillon, and K. Joulain, *Phys. Rev. Applied* **6**, 054003 (2016).
- [31] K. Joulain, Y. Ezzahri, J. Drevillon, and P. Ben-Abdallah, *Appl. Phys. Lett.* **106**, 133505 (2015).
- [32] P. Ben-Abdallah and S.-A. Biehs, *Phys. Rev. Lett.* **112**, 044301 (2014).
- [33] R. Bosisio, S. Valentini, F. Mazza, G. Benenti, R. Fazio, V. Giovannetti, and F. Taddei, *Phys. Rev. B* **91**, 205420 (2015).
- [34] Y. Zhang, X. Zhang, Z. Ye, G. Lin, and J. Chen, *Appl. Phys. Lett.* **110**, 153501 (2017).
- [35] B.-Q. Guo, T. Liu, and C.-S. Yu, *Phys. Rev. E* **99**, 032112 (2019).
- [36] Y. Zhang, Z. Yang, X. Zhang, B. Lin, G. Lin, and J. Chen, *Europhys. Lett.* **122**, 17002 (2018).
- [37] B.-Q. Guo, T. Liu, and C.-S. Yu, *Phys. Rev. E* **98**, 022118 (2018).
- [38] R. Ghosh, A. Ghoshal, and U. Sen, *Phys. Rev. A* **103**, 052613 (2021).
- [39] M. T. Naseem, A. Misra, O. E. Müstecaplıoğlu, and G. Kurizki, *Phys. Rev. Research* **2**, 033285 (2020).
- [40] M. G. Floquet, *Ann. ENS* **12**, 47 (1883).
- [41] S. Mondal, S. Bhattacharjee, and A. Dutta, *Phys. Rev. E* **102**, 022140 (2020).
- [42] R. Alicki, D. Gelbwaser-Klimovsky, and G. Kurizki, *arXiv:1205.4552*.
- [43] R. Kosloff, *Entropy* **15**, 2100 (2013).
- [44] R. Kosloff and A. Levy, *Annu. Rev. Phys. Chem.* **65**, 365 (2014).
- [45] R. Alicki, *Open Syst. Inf. Dyn.* **21**, 1440002 (2014).
- [46] H. Spohn, *J. Math. Phys.* **19**, 1227 (1978).
- [47] J. Millman, C. Halkias, and C. D. Parikh, *Integrated Electronics* (McGraw-Hill, New York, 2009).
- [48] D. Gelbwaser-Klimovsky, R. Alicki, and G. Kurizki, *Phys. Rev. E* **87**, 012140 (2013).
- [49] B. Karimi and J. P. Pekola, *Phys. Rev. B* **94**, 184503 (2016).
- [50] T. B. Batalhão, A. M. Souza, L. Mazzola, R. Auccaise, R. S. Sarthour, I. S. Oliveira, J. Goold, G. De Chiara, M. Paternostro, and R. M. Serra, *Phys. Rev. Lett.* **113**, 140601 (2014).
- [51] J. Ordonez-Miranda, Y. Ezzahri, J. Drevillon, and K. Joulain, *J. Appl. Phys.* **119**, 203105 (2016).
- [52] J. Ordonez-Miranda, Y. Ezzahri, J. A. Tiburcio-Moreno, K. Joulain, and J. Drevillon, *Phys. Rev. Lett.* **123**, 025901 (2019).
- [53] H. Carmichael, *Statistical Methods in Quantum Optics I: Master Equations and Fokker-Planck Equations*, Physics and Astronomy Online Library (Springer, Berlin, 1999).
- [54] H.-P. Breuer and F. Petruccione, *The Theory of Open Quantum Systems* (Oxford University Press, Oxford, 2002).
- [55] R. T. Wijesekara, S. D. Gunapala, M. I. Stockman, and M. Premaratne, *Phys. Rev. B* **101**, 245402 (2020).
- [56] K. Szczygielski, D. Gelbwaser-Klimovsky, and R. Alicki, *Phys. Rev. E* **87**, 012120 (2013).
- [57] D. Gelbwaser-Klimovsky, K. Szczygielski, U. Vogl, A. Saß, R. Alicki, G. Kurizki, and M. Weitz, *Phys. Rev. A* **91**, 023431 (2015).